

GISR: Geometric Initialization and Silhouette-based Refinement for Single-View Robot Pose and Configuration Estimation

Ivan Bilić¹, Filip Marić^{1,2}, Fabio Bonsignorio¹ and Ivan Petrović¹.

Abstract—For autonomous robotics applications, it is crucial that robots are able to accurately measure their internal state and perceive their environment, including other agents within it (e.g., cobots interacting with humans). The redundancy of these measurements is important, as it allows for planning and execution of recovery protocols in the event of sensor failure or external disturbances. Visual estimation can provide this redundancy through the use of low-cost sensors and serve as a standalone source of proprioception when no encoder-based sensing is available. Therefore, we estimate the configuration of the robot jointly with its pose, which provides a complete spatial understanding of the observed robot. We present GISR - a method for deep configuration and robot-to-camera pose estimation that prioritizes real-time execution. GISR is comprised of two modules: (i) a geometric initialization module, efficiently computing an approximate robot pose and configuration, and (ii) an iterative silhouette-based refinement module that refines the initial solution in only a few iterations. We evaluate our method on a publicly available dataset and show that GISR performs competitively with existing state-of-the-art approaches, while being significantly faster compared to existing methods of the same class. Our code is available at <https://github.com/iwhitey/GISR-robot>.

Index Terms—Deep Learning for Visual Perception, Visual Learning, Robot Pose Estimation, Robot Configuration Estimation

I. INTRODUCTION

Robotics applications in a wide array of domains rely on accurate camera-to-robot pose and configuration measurements. In applications such as robotic grasping, finding the camera-to-robot pose is crucial, as sensor-centered measurements of interest (e.g., object detections) need to be transformed to the robot’s reference frame [1]. Once spatial analysis in the context of the task is complete, the robot is set in motion using control algorithms that rely on accurate proprioceptive sensing from joint encoders. However, robots that operate in hazardous environments (e.g., nuclear decommissioning) or perform strenuous tasks (e.g., heavy loading) often lack proprioceptive sensors [2]. Similarly, failure in proprioceptive sensing may be detrimental in applications where robots perform tasks in environments not easily accessible to humans (e.g., underwater welding [3]), incurring high operational delay and maintenance expenses. Redundancy offered by additional proprioceptive estimates

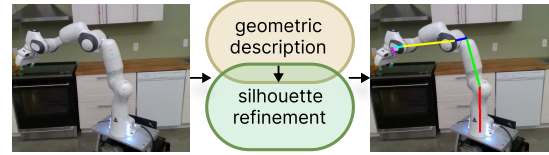


Fig. 1: GISR takes an input RGB image of the robot (left) and outputs an estimate of both the camera-to-robot pose and the configuration of the robot. The corresponding skeleton is projected onto the input image and overlaid (right).

allows for the design of recovery protocols that could help avoid many consequences of system failure. Moreover, the ability to jointly estimate the robot pose and configuration using visual cues can be of great value in scenarios with dynamic and unstructured environments, improving collaboration between robots [4] and enhancing safety in human-robot collaboration [5].

We consider the estimation of both the 6D camera-to-robot pose and the the robot’s joint angle values (i.e., configuration), using a single RGB image as input, as shown in Fig. 1. The use of off-the-shelf cameras for image-based estimation of robot configurations is cost-effective in terms of hardware, provides a non-invasive way to monitor robot configurations and offers a large degree of flexibility in sensor placement. Recent works have proposed methods for estimating either the camera-to-robot pose or robot configuration from a single RGB image based on keypoint detection [6], [7], [8], rendering-based refinement [9], and geometry-aware models [10], demonstrating favorable performance compared to classical marker-based approaches. For example, keypoint-based methods [6], [7], [8], [10] can recover the 6D pose or configuration in real-time, but require ground-truth configuration or exhibit very limited accuracy. Conversely, rendering-based methods [9] can recover both, but their dense and iterative nature incurs a high computational cost to do so very accurately.

In this paper, we present GISR - a method that can recover camera-to-robot-pose and configuration estimates in real-time using a strong geometric prior and dense silhouette-based refinement. GISR leverages the expressive power of Deep Neural Networks (DNNs) and a geometric prior associated with the robot’s kinematic model to realize two modules that complement each other. The geometric initialization module (GIM) produces an initial estimate of the camera-to-robot pose and robot configuration using the distance-geometric model introduced in [11], [12]. Using this initial estimate, the refinement module (RM) generates

*This work has been supported by the H2020 project AIFORS under Grant Agreement No 952275

¹Department of Control and Computer Engineering, Faculty of Electrical Engineering and Computing, University of Zagreb, Croatia (name.surname@fer.hr). Ivan Bilić is the corresponding author (ivan.bilic@fer.hr)

²University of Toronto Institute for Aerospace Studies, Canada. (filip.marić@mail.utoronto.ca)

a corresponding silhouette image, which is used alongside the segmented input image to predict an update. Assuming known camera intrinsics, we posit that a rendered silhouette of the robot contains most information essential for the joint estimation task. Moreover, excluding RGB image details like background and lighting helps avoid the fidelity gap due to rendering imperfections and environment variations. Therefore, using silhouette images simplifies learning by focusing only on critical information, offering faster rendering and reduced fidelity discrepancies.

Unlike similar methods that focus on only one aspect, GISR is able to recover both the camera-to-robot pose and joint configuration. Our implementation of GISR exhibits a running time in the order of 40ms, which is $20\times$ faster than existing dense methods and comparable to the speed of keypoint-based methods that rely on ground-truth configuration measurements. We provide a quantitative and qualitative analysis of our approach on a high-DoF robot using a publicly available dataset.

II. RELATED WORK

A. Object pose estimation

Estimating the 6D pose of rigid objects from a single RGB image is a long-standing goal in computer vision. Most relevant to our work are pose estimation approaches based on keypoint detection and refinement. Within the keypoint-based approach, state-of-the-art methods [13], [14], [15] train DNNs to detect object features in an image and establish a sparse set of 2D-3D correspondences. The camera pose is then recovered using the Perspective-n-Point (PnP) algorithm [16] acting on the correspondences. These methods are usually fast but less robust as they determine the pose from a sparse data. Further, various methods use a refinement-based approach that iteratively improves the pose prediction by directly regressing the pose updates [17], [18] or optimizing over dense features extracted from the DNNs [19]. These methods are typically more robust, but also more computationally intensive compared to the those using the keypoint-based approach. Overall, camera-to-object and camera-to-robot pose estimation are two closely related problems, since a robot manipulator can be considered as a complex object with multiple degrees of freedom. Therefore, our refinement module is inspired by methods that iteratively generate images representing estimated quantities and learn the residuals through implicit comparison with a reference image [9], [17], [18].

B. Camera-to-robot pose estimation

Camera-to-robot pose estimation is essential for many robotic applications, e.g., collaborative robotics [4], augmented reality [20] and robotic surgery [21], to name a few. The classical approach to determine the camera-to-robot pose, known as hand-eye calibration [22], is based on the use of multiple frames and fiducial markers [23]. More recently, single-view RGB methods, largely influenced by ideas from object pose estimation, have started gaining traction in the robotics research community. In [6], [20],

DNNs are trained to predict a set of keypoints associated with the 2D joint positions of the robot, while their 3D correspondences are found by applying forward kinematics using the known current configuration of the robot. At test time, the PnP algorithm is then applied to solve for the pose using the established 2D-3D correspondences. In [7], the PnP algorithm is integrated into the learning process to train a keypoint detector in a self-supervised manner. However, keypoint-based methods are less robust to viewpoint changes [9] and can be affected by a suboptimal specification of keypoint locations [24]. In the context of soft robotics, [25] use a differentiable renderer to create a richer, spatially-informed cost function for an optimization-based alignment of geometric primitives. Similarly, the authors of [9] employ rendering-based refinement detached from the learning process for joint camera-to-robot pose and configuration estimation, resulting in a model that is more robust compared to keypoint-based methods. Borrowing from both approaches, GISR uses a deep refinement module preceded by a geometric module based on [10], which learns to generate initial estimates by minimizing a loss that jointly encodes the robot configuration and kinematic structure.

C. Joint camera-to-robot pose and configuration estimation

Jointly estimating the 6D camera-to-robot pose and the robot configuration offers a wider range of applications compared to pose-only or configuration-only estimation, at the cost of greater complexity due to a lack of ground-truth spatial information. Learning to estimate both quantities may also help increase overall robustness by making the model rely on structural information such as link geometry, while carrying a potentially higher risk of overfitting when the data is insufficient or badly distributed. Recently, several frameworks have been proposed that solve this or similar problems using only a single RGB image as an input. In [8], the authors propose to train a keypoint detector followed by local optimization, detached from the learning process, to directly regress the full state of a low-cost 4-DoF manipulator. Similarly, Labbé et. al [9] propose a method inspired by DeepIM [17], where rendered RGB images of the robot model at an estimated pose and configuration are used as inputs to the refinement module. Each refinement stage starts from a fixed initialization and updates the pose and joint angles to minimize the configuration error, as well as the distance between point clouds corresponding to specific robot segments selected at each iteration according to a predefined schedule.

In contrast, the GISR refinement module uses a rendered silhouette of the robot at the previous configuration estimate and the segmented input image to produce an update minimizing the 3D joint position error. In this way, the refinement module learns the distribution of initial estimates produced by the trainable geometric module, reducing the discrepancy between initialization applied at train and test times. The silhouette images are generated using a fast rendering procedure without using rasterization and shading, which results in a total running time almost 20 times lower

than [9].

III. PROPOSED METHOD

Given an input RGB image of the robot manipulator comprised of a series of rigid links and revolute joints, our goal is to recover the observed robots' configuration $\mathbf{q} \in \mathcal{C}$, where $\mathcal{C} \subseteq \mathbb{R}^n$ represents the configuration space, and a 6D camera-to-robot pose ${}^c_b\mathbf{T}$ consisting of a rotation $\mathbf{R} \in SO(3)$ and a translation $\mathbf{t} \in \mathbb{R}^3$ with respect to the camera coordinate frame. As shown in Fig. 2, GISR consists of a geometric initialization module and a refinement module, which are described in detail throughout this section.

A. Geometric initialization module

The proposed geometric initialization method enables a fast computation of an informed initial guess of the robot pose \mathbf{T} and the configuration Θ observed in an image \mathcal{I} . To achieve this, our initialization procedure exploits insights from recent work on distance-based inverse kinematics [10], [11], which show that the configuration of a robot whose kinematic model $\Theta = \{\theta_0, \theta_1, \dots, \theta_n\}$ is known can be recovered from spatial constraints arising from a set of 3D points $\mathcal{X} = \{\mathbf{P}, \mathbf{Q}\}$ defined with respect to the robot's kinematic chain. More specifically, these 3D points are given by:

$$\begin{aligned} \mathbf{p}_i &= C \prod_{j=1}^i {}^{j-1}\mathbf{T}(\theta_j) \\ \mathbf{q}_i &= \mathbf{p}_i + \mathbf{R}_i \hat{\mathbf{z}}, \end{aligned} \quad (1)$$

where the joint positions \mathbf{P} are extracted by applying a selection matrix C to the computed pose transformations for the coordinate frame $i \in \{1, \dots, n\}$ of each link, while the points \mathbf{Q} are defined to be a unit distance away from points \mathbf{P} along the joints' rotation axes $\hat{\mathbf{z}}$ using their respective orientation \mathbf{R}_i . Instead of recovering the points directly, the task of the geometric module is formulated as recovering the Euclidean Distance Matrix (EDM) that these points generate:

$$\mathbf{D}^* = \arg \min_{\mathbf{D}} \|\hat{\mathbf{D}}(\mathcal{K}, \zeta) - \mathbf{D}(\Theta^*)\|_F, \quad (2)$$

where $\|\cdot\|_F$ represents Frobenius norm, \mathcal{K} denotes a set of 2D keypoints representing the coordinate frame positions of the joints, as defined by the kinematic model of the robot, and ζ is parametrized by a shallow feedforward neural network. $\mathbf{D}(\Theta^*)$ represents a target distance matrix constructed from points defined in (1), which uniquely corresponds to the ground-truth configuration Θ^* and serves as a geometric description of the robot configuration observed in the image. Prior to recovering the observed configuration, the set of points corresponding to the estimated $\hat{\mathbf{D}}$ is determined via multidimensional scaling (MDS) by solving an optimization problem:

$$\mathcal{X} = \arg \min_{\mathbf{x}_1, \dots, \mathbf{x}_n} \sum_{i < j} (\|\mathbf{x}_i - \mathbf{x}_j\| - d_{ij})^2, \quad (3)$$

which in our case has an analytic solution given via eigen-decomposition [26]. The observed configuration is finally recovered by applying a set of kinematic transformations to \mathcal{X} as described in [11], essentially by extracting coordinate frame positions and rotation axes with respect to the robot's zero position. These transformations are differentiable and referred to as inverse kinematics (IK) layer, since they map spatial constraints to the robot configuration. Together with distance matrix regression (2) and a MDS layer (3), they form an end-to-end trainable geometric pipeline that predicts an initial solution for the observed configuration.

To estimate the initial 6D robot-to-camera pose ${}^c_b\mathbf{T}$, we first use (1) to compute 3D joints' positions from the initial configuration. Then, assuming known camera intrinsics and estimated 2D keypoints, we establish 2D-3D correspondences and apply the Efficient Perspective-n-Point algorithm (EPnP) [16]. Any keypoint detector trained to follow the specifications of the robot's coordinate frames can be used to determine the keypoints. If we assume that the keypoints are perfectly detected, the pose and configuration estimated in this manner are tightly coupled, i.e., the error in the estimated pose is completely determined by the error in the estimated configuration. To alleviate this effect, we approximate the translational component of ${}^c_b\mathbf{T}$ by using the kinematic model of the robot and the estimated keypoints, information that we already assume is available. More specifically, we compute the scaling factor $\lambda \in \mathbb{R}$ as follows:

$$\lambda = \frac{\|L_{ij}\|}{\|\tilde{\mathbf{p}}_i - \tilde{\mathbf{p}}_j\|}, \quad (4)$$

where uncalibrated 2D keypoints $\tilde{\mathbf{p}}_i, \tilde{\mathbf{p}}_j$ bound the chosen link L_{ij} of known length by representing the positions of its child and parent coordinate frames i, j . The initial translational component is defined by the scale factor, camera intrinsics, and a reference keypoint \mathbf{p}_{ref} chosen to represent the reference frame of the robot with respect to the camera. For simplicity, we choose the base frame of the robot $\mathbf{p}_{ref} = \mathbf{p}_{base}$ and use it to compute (4) together with the keypoint of the neighboring joint.

B. Refinement module

The refinement module uses the initial estimates of robot pose and configuration generated by GIM and estimates their updates based on a rendered silhouette image of the robot defined by the initial estimates. Given that robotic manipulator consists of rigid links connected in a kinematic chain, each rigid link is visually described by a separate mesh \mathcal{M}_i consisting of a set of vertices ${}^i\mathcal{V} = \{\nu_0, \nu_1, \dots, \nu_n\}$ defined in the local coordinate frame of the i -th link. To render an image, the meshes must be connected to form a continuous chain by transforming each vertex ${}^i\nu \in \mathbb{R}^3$ via respective link-to-base rigid transformation:

$${}^b\tilde{\nu} = {}^b_i\mathbf{T}(\Theta) {}^i\nu, \quad (5)$$

where ${}^b_i\mathbf{T}(\Theta) \in SE(3)$, parametrized by robot configuration, is obtained from forward kinematics and transforms the vertices into the base coordinate system of the robot. To generate

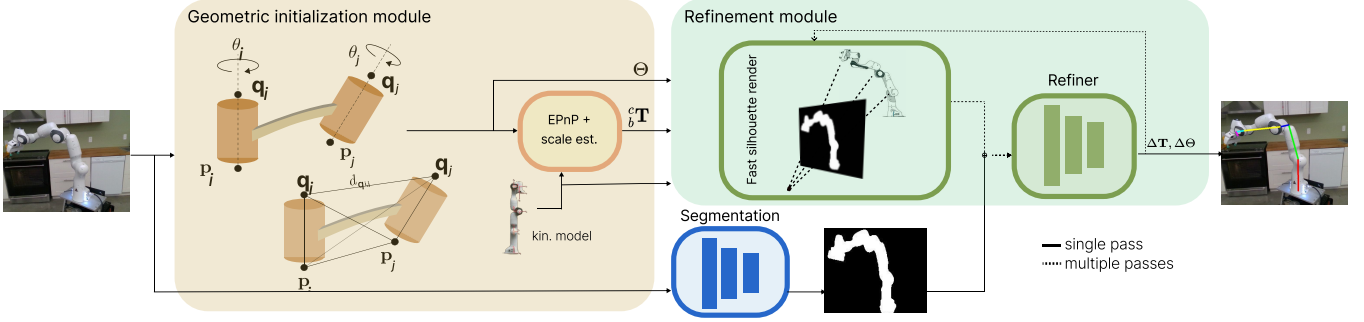


Fig. 2: System overview. The geometric initialization module (GIM) takes an input RGB image and produces initial estimates of the robot pose and configuration. The refinement module (RM) uses these estimates to generate a corresponding silhouette image, which is fed to the refiner along with the segmented input image to predict an update. This render-and-update process can be repeated, but each iteration requires a forward pass of a deep model (including the update and rendering).

a silhouette image \mathbb{S} representing the initial estimates of the camera-to-robot pose ${}^c_b\mathbf{T}_{init}$ and configuration Θ_{init} , points from the robot mesh \mathcal{M} are first sampled uniformly. These points are then transformed into the camera frame using the estimated pose ${}^c_b\mathbf{T}$, and projected onto the image plane:

$$\mathbb{S} = \pi(\mathcal{M}, {}^c_b\mathbf{T}, \mathbf{K}), \quad (6)$$

where $\pi(\cdot)$ is the projection operator, while \mathbf{K} represents the camera intrinsics.

Next, an input RGB image is converted into a silhouette image, concatenated with the rendered silhouette and fed to a deep neural network that outputs an update $\Delta\Theta, \Delta\mathbf{T}$. The configuration is updated by summation:

$$\hat{\Theta} = \Theta_{init} + \Delta\Theta, \quad (7)$$

whereas the update of the pose $\Delta\mathbf{T} = \{\Delta\mathbf{R}, \Delta\lambda\}$ is decomposed into multiplicative updates of the rotation matrix and the scaling factor:

$$\begin{aligned} {}^c_b\hat{\mathbf{R}} &= \Delta\mathbf{R} {}^c_b\mathbf{R}_{init} \\ \hat{\lambda} &= \Delta\lambda \lambda_{init}. \end{aligned} \quad (8)$$

The relative pose ${}^c_b\hat{\mathbf{T}}$ is defined by the updated rotation matrix ${}^c_b\hat{\mathbf{R}}$ parametrized according to [27], and the translation $\hat{\mathbf{t}} = \hat{\lambda}\mathbf{K}^{-1}\mathbf{p}_{base}$ computed by back-projecting the 2D detection of the robot's reference frame \mathbf{p}_{base} . Thus, the estimated rotation is decoupled from the translation, which in turn is decomposed into respective keypoint and distance estimates. It is known that estimating the translation in this way is simpler than direct regression [28].

The model is trained in a supervised manner to predict the pose and configuration updates. Before calculating the configuration loss, we project the predicted configuration via basic trigonometric functions to account for angular rotation, since the range of joint motion is in the $[0, 2\pi]$ interval. We therefore compute $\hat{\mathbf{A}} = [\sin(\hat{\Theta}) \oplus \cos(\hat{\Theta})]$, where $\hat{\mathbf{A}} \in \mathbb{R}^{2n}$ is obtained by concatenation \oplus of $\sin(\cdot)$ and $\cos(\cdot)$, which act on the configuration element-wise. The configuration loss is then:

$$\mathcal{L}_c = |\hat{\mathbf{A}} - \mathbf{A}|, \quad (9)$$

where $|\cdot|$ is the L_1 norm. Furthermore, we compute the pose loss by comparing the ground-truth and estimated 3D joint positions defined in the camera frame and obtained by applying the estimated and ground truth pose transformations, respectively:

$$\mathcal{L}_p = |(\hat{\mathbf{R}}, \hat{\mathbf{t}})\mathbf{P} - (\mathbf{R}, \mathbf{t})\mathbf{P}| + |(\mathbf{R}, \hat{\mathbf{t}})\mathbf{P} - (\mathbf{R}, \mathbf{t})\mathbf{P}|, \quad (10)$$

where \mathbf{P} is computed using forward kinematics and (\mathbf{R}, \mathbf{t}) is the ground-truth pose. Following [9], we use the two different terms to separate the influence of each estimate $\hat{\mathbf{R}}, \hat{\mathbf{t}}$ on the estimated pose, although we only use a sparse set of 3D joint positions compared to a random sample of pose anchors. The final loss is a linear combination of (9) and (10). Instead of individual loss weighting, we normalize the gradients w.r.t. output layers to a unit norm to encourage equal contribution of different losses in the shared latent space.

To summarize, instead of using random perturbations of the ground truth as initial estimates during training, we use a trainable geometric initialization module, employing the same setup during test time. Consequently, the initialization of the refinement module will be closer to a true solution, resulting in a lower running time and more accurate estimates. Equally important, we employ a fast rendering procedure without using rasterization and shading to generate silhouette images of the robot, which we use to train the refiner.

IV. EXPERIMENTAL RESULTS

In this section, we present our experimental results and provide ablations using both real and synthetic data. Specifically, we investigate how the GISR's initialization and refinement modules contribute to the robot pose and configuration estimates, and we examine their impact on the training and running time. We also analyze how the predictions of the refinement module depend on the availability of varying information from the geometric initialization module and different training data sizes. Further, we examine the effectiveness of a simple, yet important feature of our method - learning from fast-to-generate silhouette images instead of rendering RGB images via off-the-shelf rendering pipelines. Finally, we compare GISR with existing state-of-the-art algorithms.

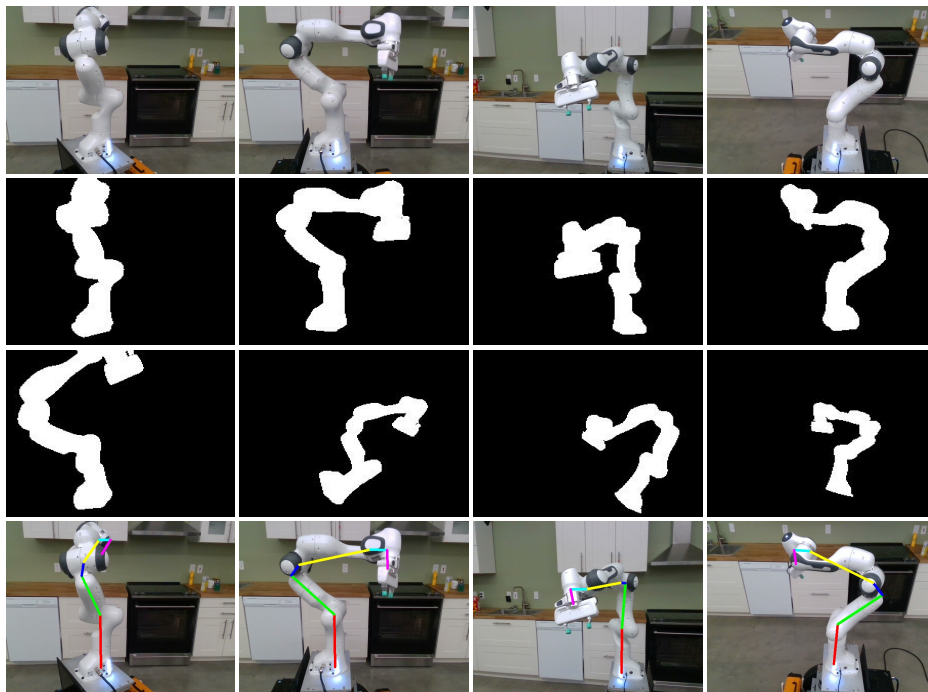


Fig. 3: Qualitative results for pose and configuration estimation, shown as a projection of the skeleton corresponding to the final estimates on the input image (last row), rendered silhouette corresponding to the initial estimate (third row), segmented input image (second row), and input image (first row).

A. Dataset and evaluation metrics

In all experiments, we used a publicly available Panda-3Cam dataset presented in [6]. The dataset contains both real and synthetic images showing a 7-DoF Franka’s Panda robotic arm in different configurations and camera-to-robot poses. The synthetic part of the dataset consists of 100k images, while the real part consists of 50k images and is divided into four parts; Azure (AK), Kinect (XK), RealSense (RS), and ORB datasets captured using three different cameras. Robot pose and configuration estimates are evaluated using the average Euclidean distance (ADD) metric:

$$ADD = \frac{1}{n} \sum_{i=1}^n \left\| {}^c\mathbf{T}\mathbf{p}_i - {}^c\hat{\mathbf{T}}\hat{\mathbf{p}}_i \right\|, \quad (11)$$

where ${}^c\mathbf{T}$ and \mathbf{p}_i denote the ground-truth camera-to-robot pose and the 3D robot joint keypoints, respectively. The pose and configuration estimates are evaluated together via ADD, since $\hat{\mathbf{p}}_i$ is determined by the estimated configuration and computed using forward kinematics. We also report the area-under-the-curve (AUC) value, which is an aggregate measure of performance and indicates the percentage of predictions with ADD smaller than a given threshold.

B. Training and implementation details

GISR consists of two trainable modules; geometric initialization (GIM) and refinement (RM) modules. First, we train a shallow, three-layer MLP that performs distance matrix regression as a part of the GIM. The rest of this model (i.e., cMDS and IK layers) is differentiable and parameter-free,

so that the model comprises only 350k trainable parameters. Next, we train the RM with initializations generated by the frozen GIM, but whose dropout remains active, making the outputs of the GIM non-deterministic, which improves the generalization capability of the refiner by mimicking test time. For the RM, we use a ConvNext-Tiny backbone initialized with ImageNet weights [29], and train it on 100k synthetic examples to compare it with existing state-of-the-art methods or different sets of real data for other experiments. The input images are downsampled from a resolution of 640×480 to 224×224 to speed up training and inference. The number of refinement iterations is incremented during training upon reaching 25% and 50% of the total training iterations. Both models are trained using a batch size of 32, linear warm-up phase for the first 5% of training iterations, and the Adam optimizer. For experiments on silhouette-based refinement, input images are segmented at runtime by a pre-trained deeplabv3 [30], which is fine-tuned on 30k samples of the Panda-ORB by using the silhouette images rendered as described in Section III-B for supervision. The entire pipeline is implemented to fully utilize GPUs and batching [31], without using *for* loops (e.g., for mesh related transformations). Since training a keypoint detector is beyond the scope of this paper, the 2D keypoint annotations are randomly perturbed by Gaussian noise with a mean of zero and a variance of 30 pixels.

C. Initialization vs. refinement

In general, GIM and RM can be used individually, as both are able to predict the camera-to-robot pose and configura-

Module	Running time (s)	ADD (m)		
		AK	RS	XK
<i>init only</i>	0.034	0.159	0.227	0.238
<i>refine only</i>	0.049	0.061	0.107	0.073
<i>init & refine</i>	0.049*	0.055	0.076	0.050
<i>init* & refine</i>	0.049*	0.050	0.064	0.052

TABLE I: Module-wise ablation using ADD (m) for evaluation (lower is better) on Panda-3Cam datasets. Using the GIM and RM together leads to better performance. The best results are obtained when the RM is trained on outputs generated by the GIM, while using the same setting during test time. *Note*: the combined *init & refine* running time is not the sum of the individual times, given that the two processes can run in parallel.

tion. However, GISR uses both modules complementarily to achieve superior results, as shown in Table I. To test this idea, we trained GIM and RM both separately and together on 16k real samples, using the ADD metric for evaluation. The GIM predicts a geometric description of the robot, which is used to recover the configuration, while EPnP and forward kinematics are used to compute the 6D pose estimate (*init only*). Although the error in the order of 20 cm disqualifies it as a standalone solution, its computational efficiency makes it a suitable initialization method. On the other hand, rendering-based RM trained using random perturbations of the pose and configuration labels (*refine only*) performs better as a standalone solution - a dense method that uses images of the robot as information-rich inputs, but is also more computationally intensive. However, when used together (*init & refine*), the error decreases by 24% on average. In this setup, we trained RM as in (*refine only*), and used GIM only for initialization during test time. This shows that GIM, even though trained separately, can be used out-of-the-box to improve the performance of a pre-trained RM. The best performance is achieved when the RM is trained based on the results generated by the GIM and the same setting is used during test time (*init* & refine*). This is due to two related reasons. First, during training, the RM can learn to adapt to the output distribution of the GIM and make larger corrections to the predicted pose and configuration for samples where the GIM produces larger errors, as opposed to training using random ground-truth perturbations where recurrent or similar states are perturbed by different error magnitudes. Second, the same initialization procedure is used at test time, which serves as a geometric prior and reduces the discrepancy that occurs in the (*refine only*) and (*init & refine*) setups, where the initialization strategies used at train and test times differ, simply due to the lack of information at test time.

D. Varying initial information

In the following, we investigate how varying the initial information about the observed robot by excluding different components of the GIM affects the final performance and

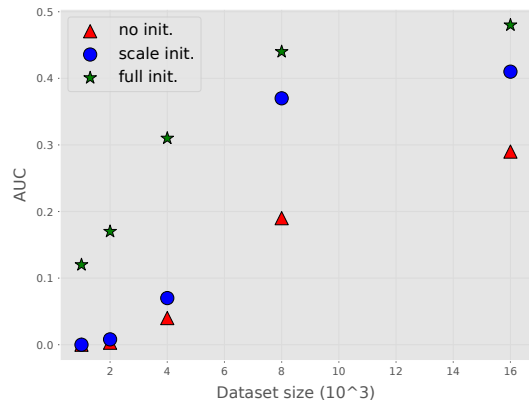


Fig. 4: AUC score as a function of training data size for different initialization schemes; (i) fixed initialization, i.e., no prior information about the observed robot (*no init.*), (ii) initializing scale using 2D keypoints and known robot DH parameters (*scale init.*) and (iii) initializing configuration, scale, and rotation, which amounts to full use of the GIM.

scalability of GISR with real training data, especially for small to medium data sets. The results are shown in Fig. 4. Different model variants are created by incrementally adding new information to the initial estimate, trained using different amounts of data and evaluated using the AUC score. The first variant (*no init.*) is a pure refinement model that is trained using random perturbations of the ground truth to simulate a scenario without prior information, and evaluated using a fixed initialization; unit scaling factor, rotation that aligns the camera frame to the robot base frame, and a configuration that corresponds to the middle of the joint limits. This model serves a baseline. In the second variant (*scale init.*), 2D joint keypoints and known robot DH parameters are included, enabling initialization of the scale factor used during both train and test time. In the last variant (*full init.*), we fully utilize the GIM by including robot configuration estimation and EPnP-based rotation estimation, and use the same strategy during both train and test times. All variants scale similarly, except for small amounts of training data where (*no init.*) scales slower. However, the (*full init.*) variant is clearly the best-performing across all training data sizes. In addition, the model exhibits greater sensitivity to initial scale than to rotation. This is reflected in a larger performance gain between (*no init.*) and (*scale init.*) compared to that between (*scale init.*) and (*full init.*).

E. Learning from silhouette images

Existing rendering-based methods for pose estimation of objects [17], [18] and robots [9] typically use RGB rendering. In contrast, our refinement model learns to predict the camera-to-robot pose and configuration updates based on silhouette images. We tested two approaches. In the first approach, GISR uses the reference and rendered RGB images that reflect the observation and the current estimate, respectively. In the second approach, the GISR takes the respective silhouette images as input instead, where the reference RGB

Rendering type	Train time (h)	Running time (s)	Panda-3Cam-AK	Panda-3Cam-RS	Panda-3Cam-XK
RGB	206.85	0.096	40.12	46.05	44.07
Silhouette	108.52	0.049	49.64	57.93	43.13
Silhouette*	108.52	0.016*	55.48	63.82	53.79

TABLE II: Comparison of RGB-based refinement with our silhouette-based refinement via the AUC score (higher is better). The results obtained by mimicking an ideal robot segmentation model (last row) show the possibility for further improvements. Also, the running time (*) would be higher, assuming a deep model performs the segmentation.

Method	Θ_{gt}	Running time (s)	Panda-3Cam-AK		Panda-3Cam-XK		Panda-3Cam-RS		all	
			#images = 6394		#images = 4966		#images = 5944		#images = 17304	
			AUC \uparrow	ADD (m) \downarrow	AUC \uparrow	ADD (m) \downarrow	AUC \uparrow	ADD (m) \downarrow	AUC \uparrow	ADD (m) \downarrow
DREAM-F	✓	0.042	68.912	11.413	24.359	491.911	76.130	2.077	60.740	113.029
DREAM-Q	✓	0.029	52.382	78.089	37.471	54.178	77.984	0.027	56.988	59.284
DREAM-H	✓	0.033	60.520	0.056	64.005	7.382	78.825	0.024	68.584	17.477
CtRNet	✓	0.033	89.928	0.013	79.465	0.032	90.789	0.010	85.962	0.020
RoboPose	✗	1	70.374	0.033	77.617	0.035	74.315	0.027	74.101	0.032
Ours	✗	0.049	80.613	0.022	73.941	0.039	79.324	0.021	77.959	0.027

TABLE III: Comparison with state-of-the-art methods. Evaluation protocol from existing work is followed by using an AUC with a 0.1m threshold in addition to ADD.

image is converted into a silhouette image via segmentation. The silhouette image corresponding to the current estimate is computed as described in Section III-B, which amounts to generating an image without the steps typically applied in rendering, i.e., rasterization and shading. Compared to an optimized off-the-shelf RGB renderer [31], we measure a twofold speedup in model inference and training (see Table II), which is important considering that the refinement procedure is iterative, i.e., the rendering process is repeated at each forward pass. As shown in Table II, the model trained on silhouette images outperforms its RGB counterpart (+9.52 increase in AUC for Panda-3Cam-AK, and +11.88 for Panda-3Cam-RS).

Assuming that the camera intrinsics and the 3D model of the robot are known, a silhouette image of the robot is completely defined by its configuration and the camera-to-robot pose and thus contains all necessary information for the model to learn, while omitting irrelevant details present in RGB images. In the context of our task, only a small subset of information present in RGB images provides additional value for generalization (e.g., salient color patterns on the robot), thereby making the model more susceptible to overfitting, as it must learn to ignore most of it (e.g., background, lighting conditions). Similarly, RGB-based methods are more affected by the fidelity gap between input and rendered images, due to imperfections in the rendering process and the 3D model of the robot, as well as variations in background and lighting conditions. Therefore, using silhouette images to learn the camera-to-robot pose and configuration is a simple and effective feature that limits the model to focus only on the information that is most important for recovery, with a faster rendering time and a lower discrepancy in fidelity, but at the cost of an additional model.

The last row in Table II shows how the performance of

the robot segmentation affects the camera-robot pose and configuration estimation. To measure this, we conducted evaluation by generating a silhouette image that corresponds to the input image using the exact same procedure used for silhouette rendering, which simulates the scenario of an "ideal" segmentation model during test time. The results clearly show that improving the segmentation model alone results in much more accurate estimates of camera-robot pose and configuration. It should be noted that this does not require human annotations at the pixel level, which are commonly used to train segmentation models, as we use the described simplified silhouette rendering technique to supervise the model and utilize the actual robot configuration and camera-robot pose, which are less time consuming and easier to capture.

F. Comparison to state-of-the-art methods

Here we present the evaluation of our method in comparison to the existing state-of-the-art methods. The results are shown in Table III. DREAM [6] and CtRNet [7] belong to the class of keypoint-based methods and recover only 6D camera-to-robot pose, for which they require ground-truth configuration at test time (Θ_{gt}). In contrast, RoboPose [9] is an RGB rendering-based method trained to recover both the robot pose and the configuration, similar to our refinement model. Category-wise, our method is hybrid - we use sparse information to generate an initial solution, followed by dense silhouette-based refinement to arrive at a final solution. As reported by authors, DREAM and RoboPose were trained using only synthetic data, i.e., 100k synthetic samples [6]. To ensure a fair comparison, we trained our refinement model using the same dataset. DREAM-H, the best-performing among the DREAM variants, is outperformed by our method on each of the individual datasets, on average by +9.375 AUC. Although CtRNet outperforms our method

(+0.0076 ADD, +8.003 AUC), it still uses the ground-truth configuration at test time, while our model predicts both quantities. Also, note that CtrNet was trained on real Panda-3Cam datasets, in addition to synthetic pre-training [7]. Our approach significantly outperforms RoboPose on two out of three datasets (+10.24 on 3Cam-AK, +5.01 on 3Cam-RS) and on average by 3.86 AUC, except on the 3Cam-XX dataset (-3.68 AUC). To achieve these results, RoboPose uses 10 refinement iterations, i.e., 10 model forward passes. Our refinement model not only uses a fast, simplified silhouette rendering, but also uses only 3 iterations. This makes our method 20× faster while achieving better results. In terms of performance, our method is competitive with keypoint-based methods that use ground-truth robot configuration.

V. CONCLUSION

In this paper, we present GISR, a novel approach to jointly estimate camera-to-robot pose and configuration by utilizing both sparse and dense information. Our architecture uses distinct geometric initialization and refinement modules to accurately estimate both quantities, which enables improving the final performance by fine-tuning specific subtasks. The proposed silhouette-based refinement can be executed with low computation times, making it suitable for online estimation and dynamic scenarios with mobile robots. However, the use of multiple modules also increases the overall complexity and memory requirements compared to end-to-end approaches. For future work, we consider extending this approach to unknown robots, i.e., to discover their kinematic model.

REFERENCES

- [1] J. Tremblay, S. Tyree, T. Mosier, and S. Birchfield, "Indirect object-to-robot pose estimation from an external monocular rgb camera," in *2020 IEEE/RSJ International Conference on Intelligent Robots and Systems (IROS)*. IEEE, 2020, pp. 4227–4234.
- [2] V. Ortenzi, N. Marturi, M. Mistry, J. Kuo, and R. Stolkin, "Vision-based framework to estimate robot configuration and kinematic constraints," *IEEE/ASME Transactions on Mechatronics*, vol. 23, no. 5, pp. 2402–2412, 2018.
- [3] M. K. Maity, S. Suman, and P. Biswas, "Autonomous robotic underwater welding—a review." Springer Nature Singapore, 2023.
- [4] F. Caccavale and M. Uchiyama, "Cooperative manipulation," *Springer handbook of robotics*, pp. 989–1006, 2016.
- [5] R.-J. Halme, M. Lanz, J. Kämäräinen, R. Pieters, J. Latokartano, and A. Hietanen, "Review of vision-based safety systems for human-robot collaboration," *Procedia CIRP*, vol. 72, pp. 111–116, 2018, 51st CIRP Conference on Manufacturing Systems.
- [6] T. E. Lee, J. Tremblay, T. To, J. Cheng, T. Mosier, O. Kroemer, D. Fox, and S. Birchfield, "Camera-to-robot pose estimation from a single image," in *2020 IEEE International Conference on Robotics and Automation (ICRA)*. IEEE, 2020, pp. 9426–9432.
- [7] J. Lu, F. Richter, and M. C. Yip, "Markerless camera-to-robot pose estimation via self-supervised sim-to-real transfer," in *Proceedings of the IEEE/CVF Conference on Computer Vision and Pattern Recognition*, 2023, pp. 21 296–21 306.
- [8] Y. Zuo, W. Qiu, L. Xie, F. Zhong, Y. Wang, and A. Yuille, "Craves: Controlling robotic arm with a vision-based economic system," in *2019 IEEE/CVF Conference on Computer Vision and Pattern Recognition (CVPR)*, 2019, pp. 4209–4218.
- [9] Y. Labbé, J. Carpentier, M. Aubry, and J. Sivic, "Single-view robot pose and joint angle estimation via render & compare," in *Proceedings of the IEEE/CVF Conference on Computer Vision and Pattern Recognition*, 2021, pp. 1654–1663.
- [10] I. Bilić, F. Marić, I. Marković, and I. Petrović, "A distance-geometric method for recovering robot joint angles from an rgb image," *IFAC-PapersOnLine*, vol. 56, no. 2, pp. 1003–1008, 2023, 22nd IFAC World Congress.
- [11] F. Marić, M. Giamou, A. Hall, S. Khoubyarian, I. Petrović, and J. Kelly, "Riemannian optimization for distance-geometric inverse kinematics," *IEEE Transactions on Robotics*, vol. 38, no. 3, pp. 1703–1722, 2022.
- [12] M. Giamou, F. Marić, D. M. Rosen, V. Peretroukhin, N. Roy, I. Petrović, and J. Kelly, "Convex iteration for distance-geometric inverse kinematics," *IEEE Robotics and Automation Letters*, vol. 7, no. 2, pp. 1952–1959, 2022.
- [13] G. Pavlakos, X. Zhou, A. Chan, K. G. Derpanis, and K. Daniilidis, "6-dof object pose from semantic keypoints," in *2017 IEEE International Conference on Robotics and Automation (ICRA)*, 2017, pp. 2011–2018.
- [14] B. Tekin, S. N. Sinha, and P. Fua, "Real-time seamless single shot 6d object pose prediction," in *2018 IEEE/CVF Conference on Computer Vision and Pattern Recognition*, 2018, pp. 292–301.
- [15] J. Tremblay, T. To, B. Sundaralingam, Y. Xiang, D. Fox, and S. Birchfield, "Deep object pose estimation for semantic robotic grasping of household objects," *arXiv preprint arXiv:1809.10790*, 2018.
- [16] V. Lepetit, F. Moreno-Noguer, and P. Fua, "Epnnp: An accurate o (n) solution to the pnp problem," *International journal of computer vision*, vol. 81, no. 2, pp. 155–166, 2009.
- [17] Y. Li, G. Wang, X. Ji, Y. Xiang, and D. Fox, "Deepim: Deep iterative matching for 6d pose estimation," in *Proceedings of the European Conference on Computer Vision (ECCV)*, 2018, pp. 683–698.
- [18] F. Manhardt, W. Kehl, N. Navab, and F. Tombari, "Deep model-based 6d pose refinement in rgb," in *Proceedings of the European Conference on Computer Vision (ECCV)*, 2018, pp. 800–815.
- [19] S. Iwase, X. Liu, R. Khirodkar, R. Yokota, and K. M. Kitani, "Repose: Fast 6d object pose refinement via deep texture rendering," in *Proceedings of the IEEE/CVF International Conference on Computer Vision*, 2021, pp. 3303–3312.
- [20] J. Lambrecht and L. Kästner, "Towards the usage of synthetic data for marker-less pose estimation of articulated robots in rgb images," in *2019 19th International Conference on Advanced Robotics (ICAR)*, 2019, pp. 240–247.
- [21] M. Zhou, M. Hamad, J. Weiss, A. Esлами, K. Huang, M. Maier, C. P. Lohmann, N. Navab, A. Knoll, and M. A. Nasserli, "Towards robotic eye surgery: Marker-free, online hand-eye calibration using optical coherence tomography images," *IEEE Robotics and Automation Letters*, vol. 3, no. 4, pp. 3944–3951, 2018.
- [22] R. Horaud and F. Dornaika, "Hand-eye calibration," *The International Journal of Robotics Research*, vol. 14, no. 3, p. 195–210, June 1995.
- [23] E. Olson, "Apriltag: A robust and flexible visual fiducial system," *2011 IEEE International Conference on Robotics and Automation*, pp. 3400–3407, 2011.
- [24] J. Lu, F. Richter, and M. C. Yip, "Pose estimation for robot manipulators via keypoint optimization and sim-to-real transfer," *IEEE Robotics and Automation Letters*, vol. 7, no. 2, pp. 4622–4629, 2022.
- [25] J. Lu, F. Liu, C. Girerd, and M. C. Yip, "Image-based pose estimation and shape reconstruction for robot manipulators and soft, continuum robots via differentiable rendering," *arXiv preprint arXiv:2302.14039*, 2023.
- [26] I. Dokmanic, R. Parhizkar, J. Ranieri, and M. Vetterli, "Euclidean distance matrices: Essential theory, algorithms, and applications," *IEEE Signal Processing Magazine*, vol. 32, no. 6, pp. 12–30, 2015.
- [27] Y. Zhou, C. Barnes, J. Lu, J. Yang, and H. Li, "On the continuity of rotation representations in neural networks," in *Proceedings of the IEEE/CVF Conference on Computer Vision and Pattern Recognition*, 2019, pp. 5745–5753.
- [28] Y. Xiang, T. Schmidt, V. Narayanan, and D. Fox, "Posecnn: A convolutional neural network for 6d object pose estimation in cluttered scenes," *arXiv preprint arXiv:1711.00199*, 2017.
- [29] Z. Liu, H. Mao, C.-Y. Wu, C. Feichtenhofer, T. Darrell, and S. Xie, "A convnet for the 2020s," in *Proceedings of the IEEE/CVF conference on computer vision and pattern recognition*, 2022, pp. 11 976–11 986.
- [30] L.-C. Chen, G. Papandreou, F. Schroff, and H. Adam, "Rethinking atrous convolution for semantic image segmentation," *arXiv preprint arXiv:1706.05587*, 2017.
- [31] N. Ravi, J. Reizenstein, D. Novotny, T. Gordon, W.-Y. Lo, J. Johnson, and G. Gkioxari, "Accelerating 3d deep learning with pytorch3d," *arXiv preprint arXiv:2007.08501*, 2020.